Journal of Power Sources 208 (2012) 203–209

Contents lists available at SciVerse ScienceDirect

Journal of Power Sources

journal homepage: www.elsevier.com/locate/jpowsour

Oxygen reduction reaction on a polypyrrole-modified, carbon-supported cobalt hydroxide catalyst

Hai Ying Qin, Kun Ning Zhu, Li Qiang Ye, Zhou Peng Li*

Department of Chemical and Biological Engineering, Zhejiang University, Hangzhou 310027, PR China

ARTICLE INFO

Article history:
Received 1 November 2011
Received in revised form 11 February 2012
Accepted 13 February 2012
Available online 21 February 2012

Keywords:
Oxygen reduction reaction
Polypyrrole-modified carbon-supported cobalt hydroxide
Electrocatalytic activity
Catalytic site
Cell performance

ABSTRACT

A series of polypyrrole (PPY)-modified carbon-supported $Co(OH)_2$ catalysts [$Co(OH)_2$-PPY-C] with different types of carbon supports and the PPY and $Co(OH)_2$ contents are synthesized to investigate the effect of the Co—N*x* and —C=N—C= sites on the oxygen reduction reaction (ORR). X-ray photoemission spectroscopy results reveal that the Co—N*x* and —C=N—C= sites dominate the four- and two-electron transfer ORR, respectively. The carbon support and the PPY and $Co(OH)_2$ contents of the catalysts determine the distribution of the Co—N*x* and —C=N—C= sites. The competition between these two sites determines the overall electron number of the ORR. A direct borohydride fuel cell using an optimal $Co(OH)_2$-PPY-C as the cathode catalyst exhibits a maximum power density of 550 mW cm^{-2} at 80 °C.

1. Introduction

The development of inexpensive catalysts to replace Pt in fuel cells has been an area of increasing interest in recent years. Several studies on the use of inexpensive metals [1] and macrocyclic compounds [2] as cathode catalysts for the oxygen reduction reaction (ORR) have been reported. Among these potential catalysts, carbon-supported transition metal compounds (e.g., Co/N C^{-1} and Fe/N C^{-1}) have gained increasing attention. The catalytic activity of these catalysts can be further improved by optimizing the metal precursor, ligand structure, and carbon support, as well as by heat treatment [3–5]. However, the enhancement effects of these catalysts remain unknown. A fundamental understanding of these effects would be beneficial in designing alternative and innovative catalysts for ORR [6].

ORR, is a complicated, multistep electrocatalytic reaction that occurs in aqueous alkaline media. Many species, such as OH^-, O_2^-, and HO_2^-, are proposed as important intermediates that affect ORR [7,8]. $Co(OH)_2$ and $Ni(OH)_2$ have the same hexagonal close-packed structure and similar lattice parameters. ORR occurs on the $Ni(OH)_2$/C catalyst via a four-electron reaction, but simultaneously occurs via four- and two-electron reactions on the $Co(OH)_2$/C catalyst [9]. The ORR pathway is generally classified into two categories. One involves the formation of OH^- as the final product (complete reduction, with four electrons transferred), whereas the other involves the formation of peroxide (partial reduction, with the transfer of two electrons).

Polypyrrole (PPY) modification can significantly improve the ORR kinetics on carbon-supported $Co(OH)_2$ catalysts [10–12]. A carbon support changes the electron-transfer numbers related to ORR but not to the $Co(OH)_2$ phase structure [10]. Three electrons are transferred in the catalyzed ORR on PPY-modified Super P (SP) carbon-supported $Co(OH)_2$ [$Co(OH)_2$-PPY-SP] [10,13], indicating that ORR simultaneously occurs via four- and two-electron reactions. However, ORR on PPY-modified BP2000 (BP) carbon-supported $Co(OH)_2$ [$Co(OH)_2$-PPY-BP] occurs via a four-electron reaction. The Co—N*x* (*x* = 2 or 4) and pyridinic nitrogen (—C=N—C=) sites on the Co/N C^{-1} catalysts [5,6,14,15] may be the active sites for ORR. The Co—N*x* and —C=N—C= sites are responsible for the four- and two-electron ORRs, respectively [5,6,8].

The results from previous studies [10–13] showed that PPY affects the structure, morphology, and electrocatalytic activity of PPY-modified carbon-supported catalysts. However, the effects of the interactions between nitrogen (in PPY), the transition elements, and the carbon support in $Co(OH)_2$-PPY-C on ORR remain to be determined. The present study aims to investigate the effect of the Co—N*x* and —C=N—C= sites on ORR using $Co(OH)_2$-PPY-C as the catalyst in alkaline media. A series of $Co(OH)_2$-PPY-C catalysts with different types of carbon supports and PPY and $Co(OH)_2$ contents are synthesized to vary the ratio of Co—N*x* to —C=N—C= sites in the $Co(OH)_2$-PPY-C catalysts. The effect of the catalyst composition

* Corresponding author. Tel.: +86 571 87953149; fax: +86 571 87953149.
E-mail address: zhoupengli@zju.edu.cn (Z.P. Li).

0378-7753/$ – see front matter © 2012 Elsevier B.V. All rights reserved.
doi:10.1016/j.jpowsour.2012.02.040

Table 1
Mass ratio of the raw materials used in the synthesis of the $Co(OH)_2$-PPY-BP catalysts with different polypyrrole contents.

Samples	Mass ratio of pyrrole to BP2000	Mass ratio of PPY-BP to $Co(NO_3)_2$
PPY0	0:10	3:1
PPY10	1:9	3:1
PPY20	1:4	3:1
PPY30	3:7	3:1

PPY-BP preparation condition: 10 g of carbon powder, 150 ml of glacial acetic acid solution (1.64 vol.%), volume ratio of pyrrole to H_2O_2 solution (10 wt.%) is 1:5, at 25 °C for 3 h.
$Co(OH)_2$-PPY-BP preparation condition: 3 g of PPY-BP powder, 16.64 g of $Co(NO_3)_2$ solution (6.21 wt.%), 400 mL of NaOH solution (1 wt.%), at 80 °C for 1 h.

on ORR is determined via electrochemical analysis and physical characterization.

2. Experimental details

2.1. Synthesis of the PPY-modified carbon-supported $Co(OH)_2$ composite

The preparation procedure for the PPY-modified, carbon-supported $Co(OH)_2$ composite materials was discussed in a previous study [10]. SP and BP were selected as the catalyst supports to determine the effect of the carbon support on the formation of the Co—N*x* and —C=N—C= sites. For the preparation of $Co(OH)_2$-PPY-SP and $Co(OH)_2$-PPY-BP, the mass ratio of pyrrole to carbon powder was 1:5, and that of PPY-modified carbon powder to $Co(NO_3)_2$ was 3:1. The relationship between the catalytic sites and surface composition was quantitatively analyzed via X-ray photoemission spectroscopy (XPS) by changing the relative contents of PPY and $Co(OH)_2$ on the catalyst surface. The compositions of the $Co(OH)_2$-PPY-BP catalysts are listed in Tables 1 and 2. *x* (PPY*x*) and *y* (Co*y*) represent the percentages of the PPY and Co contents in the $Co(OH)_2$-PPY-BP catalysts, respectively.

2.2. Structural characterization and elemental identification

The chemical valence states of Co and N were investigated via XPS using a PHI-5000C ESCA system (Perkin Elmer Inc., USA). All spectra were referenced to the C 1s level at 284.6 eV to correct the peak shift that occurred due to charge accumulation on the sample. Raw data were fitted using the Augerscan demo and XPSPEAK 41 software. The catalyst microstructure was observed via a JEM-2010 high-resolution transmission electron microscopy (HRTEM) operated at 200 kV.

Table 2
Mass ratio of the raw materials used in the synthesis of the $Co(OH)_2$-PPY-BP catalysts with different Co contents.

Samples	Mass ratio of pyrrole to BP2000	Mass ratio of PPY-BP to $Co(NO_3)_2$
Co0	1:5	1:0
Co5	1:5	1:0.16
Co10	1:5	1:0.33
Co15	1:5	1:0.55

PPY-BP preparation condition: 10 g of carbon powder, 150 ml of glacial acetic acid solution (1.64 vol.%), 2 ml of pyrrole, 10 ml of H_2O_2 solution (10 wt.%), at 25 °C for 3 h.
$Co(OH)_2$-PPY-BP preparation condition: 3 g of PPY-BP powder, using $Co(NO_3)_2$ solution (6.21 wt.%) and NaOH solution (1 wt.%), mass ratio of $Co(NO_3)_2$ to NaOH is 1:4, at 80 °C for 1 h.

2.3. Electrode preparation and performance

The electrochemical properties of the prepared materials were evaluated using a half-cell and a single-cell. Half-cell measurements were performed in a Zahner IM6 analyzer using the rotating disk electrode (RDE) technique. Hg/HgO and Pt-wire electrodes were used as the reference and counter electrodes, respectively. 8.0 mg of the catalyst sample, 3 mL ethanol, and 0.2 mL Nafion suspension (5 wt.%) were ultrasonically mixed to form a homogenous ink. Exactly 5 μL of the ink was then pipetted onto a pretreated glassy carbon electrode (3 mm diameter, 0.07065 cm^2 geometrical area). The electrodes were then dried at room temperature. The linear sweep voltammograms (LSVs) of the electrodes were recorded between −0.3 and 0.2 V (vs. Hg/HgO) at a scan rate of 10 mV s^{-1}. The RDE voltammograms were recorded between −1.0 and 0.2 V (vs. Hg/HgO) at a scan rate of 10 mV s^{-1} under rotation rates of 200, 400, 600, and 800 rpm in a 0.1 M KOH solution saturated with O_2 at 25 °C, respectively. All current densities were normalized to the geometric surface area of the disk electrode.

The RDE voltammograms were analyzed using the Koutecky–Levich (K–L) equation as follows [16]:

$$\frac{1}{I} = \frac{1}{I_k} + \frac{1}{0.62nFA_eC_0{D_0}^{2/3}\nu^{-1/6}\omega^{1/2}} \quad (1)$$

where I is the limiting disk current, I_k is the kinetic current, ω is the angular frequency of rotation, A_e is the electroactive area, F is Faraday constant, and n is the number of electrons transferred per O_2 molecule via ORR. The O_2 concentration (C_0), the diffusion coefficient (D_0) of O_2 in 0.1 M KOH solution, and the kinematic viscosity (ν) of the 0.1 M KOH solution are 1.15×10^{-3} M, 1.95×10^{-5} cm^2 s^{-1}, and 0.008977 cm^2 s^{-1}, respectively [17]. For a powder catalyst evaluation, use of an approximate K–L equation is a convenient way to estimate the number of electrons transferred (n), as follows:

$$\frac{1}{I} = \frac{1}{I_l} + \frac{1}{0.62nFA_gC_0{D_0}^{2/3}\nu^{-1/6}\omega^{1/2}} \quad (2)$$

where I_l stands for the kinetically limiting current, A_g is the geometric area of the disk electrode. In this study, we assume that the test catalysts have similar electroactive surface areas to evaluate the effect of the Co—N*x* and —C=N—C= sites on ORR.

The cathode in the single cell was prepared by coating the catalyst slurry onto a piece of hydrophobic carbon cloth at a catalyst loading of 5 mg cm^{-2}. The catalyst slurry was prepared by mixing the catalyst powder, deionized water, Nafion suspension (5 wt.%), and anhydrous ethanol at a mass ratio of 1:3:7:3. The anode was prepared by coating a catalyst paste onto a piece of Ni foam at a catalyst loading of 10 mg cm^{-2}. The anode catalyst paste was prepared by mixing Ni powder (INCO.210), Pt/C (5 wt.% Pt on Vulcan XC-72), and Nafion suspension (5 wt.%) at a mass ratio of 5:2:20.

A single direct borohydride fuel cell (DBFC) with an effective area of 6 cm^2 was assembled to evaluate the electrocatalytic activity of the catalysts. The cell configuration and cell test system were described in a previous study [12]. Nafion membranes N117, N112, and N211 were used as the electrolytes. An alkaline $NaBH_4$ solution (5 wt.% $NaBH_4$–10 wt.% NaOH) was used as the fuel. The cell performance was tested at 80 °C at a fuel flow rate of 50 mL min^{-1} and a humidified O_2 flow rate of 150 mL min^{-1} (0.3 MPa).

3. Results and discussion

3.1. ORR sites on $Co(OH)_2$-PPY-C with different carbon supports

Carbon support characteristics, such as disorder and microporosity, significantly affect the catalytic ORR [18]. $Co(OH)_2$ is differently distributed on the PPY-modified SP and BP because

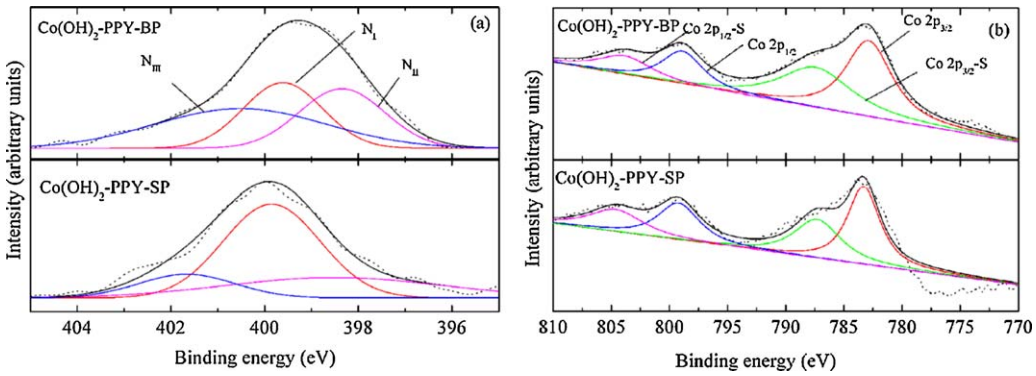

Fig. 1. X-ray photoemission spectroscopy (XPS) (a) N 1s and (b) Co 2p spectra for the $Co(OH)_2$-PPY-SP and $Co(OH)_2$-PPY-BP catalysts.

BP carbon has a larger specific surface area, lower crystallization degree, and lower electrochemical resistance than SP carbon [10]. XPS analysis of the PPY films [14,15] reveals that the binding energies of the —C=N—C= and pyrrolic (—NH—) nitrogen are 399 eV (N_I) and 400.5 eV (N_{III}), respectively. The peak at 398 eV (N_{II}) corresponds to the Co—N bond [19,20]. Fig. 1 shows the N 1s, Co $2p_{1/2}$, and Co $2p_{3/2}$ core level spectra of $Co(OH)_2$-PPY-SP and $Co(OH)_2$-PPY-BP. Three peaks (N_I, N_{II}, and N_{III}) appear in the N 1s spectrum after spectral deconvolution (Fig. 1a). The relative intensities of N_I:N_{II}:N_{III} for $Co(OH)_2$-PPY-SP and $Co(OH)_2$-PPY-BP are 4:2:1 and 3:3:4, respectively. Furthermore, the relative N surface concentration of $Co(OH)_2$-PPY-BP (1.4%) is higher than that of $Co(OH)_2$-PPY-SP (0.9%), indicating that the carbon support affects the surface nitrogen content.

Four peaks appear in the Co 2p spectrum after deconvolution (Fig. 1b), with the major peaks of Co $2p_{3/2}$ and Co $2p_{1/2}$ located at 783 and 799 eV, respectively. The binding energy of Co $2p_{3/2}$ in $Co(OH)_2$-PPY-C (783 eV) is higher than that of Co $2p_{3/2}$ (780.6 eV) in the standard $Co(OH)_2$ sample, suggesting that nitrogen binds with Co. Correlating the N_I and N_{II} peaks in the N 1s spectrum reveals that the two dominant nitrogen functional structures in $Co(OH)_2$-PPY-C are —C=N—C= and cobalt nitrogen (Co—N).

As shown in Fig. 1a, the relative proportion of the N_{II} component in $Co(OH)_2$-PPY-BP (29.7%) is equivalent to that in $Co(OH)_2$-PPY-SP (28.2%); however, the relative proportion of the N_I component in $Co(OH)_2$-PPY-BP (30.5%) is lower than that in $Co(OH)_2$-PPY-SP (57.5%). From previous results [10], the overall number of electrons (n) transferred via ORR in $Co(OH)_2$-PPY-BP and $Co(OH)_2$-PPY-SP is 3.7 and 2.9, respectively. These results imply that the Co—Nx and —C=N—C= sites may induce a four- and two-electron-dominated ORR, respectively.

3.2. $Co(OH)_2$ content of the catalyst

The N 1s, Co $2p_{1/2}$, and Co $2p_{3/2}$ core level spectra of $Co(OH)_2$-PPY-BP with different Co contents are shown in Fig. 2. Increasing the Co content does not affect the relative N surface concentration but changes the relative intensities of N_I to N_{II}. The calculated relative intensities (N_I:N_{II}) in the Co0, Co5, Co10, and Co15 samples are 1:0, 5:4, 1:1, and 3:2, respectively.

Fig. 3 shows the RDE voltammograms of the catalysts supported on the glass carbon electrode, namely, the Co0/GC, Co5/GC, Co10/GC, and Co15/GC electrodes, at rotation rates of 200, 400, 600, and 800 rpm, respectively. The K–L plots obtained from the RDE voltammograms of $Co(OH)_2$-PPY-BP with different Co contents using limiting currents at −0.6 V (Fig. 3) are shown in Fig. 4a. The relationship between the n and $-I_l$ of ORR and $Co(OH)_2$-PPY-BP with different Co contents is shown in Fig. 4b. When the Co content is increased, n rapidly increases from 1.9 to 3.9 and then becomes constant. The absolute value of I_l increases when the Co content is below 10 wt.%. However, further increase in the Co content decreases the absolute value of I_l. This result indicates that the Co content affects the reaction pathway and kinetics of ORR. The XPS results of $Co(OH)_2$-PPY-BP with different Co contents show that the —C=N—C= site drives a two-electron ORR based on the n value (1.9) of the Co0 sample. The n value of $Co(OH)_2$-PPY-BP with different Co contents coincidently changes with varying N_I and N_{II} relative intensities. Therefore, n is determined by the competition between these two catalytic sites.

Beyond a certain amount of Co content (such as the Co15 sample), the density of Co^{2+} on the catalyst surface tends to be saturated (Fig. 2b). However, selected area electron diffraction (Fig. 5) reveals that noncrystalline Co is formed, which is similar to the formation of Fe clusters worsens the Fe dispersion when the Fe content in the Cl-FeTMPP catalysts exceeds a certain value [21]. The formation of noncrystalline Co may lead to the saturation of the ORR electron-transfer number, as shown in Fig. 4b.

3.3. PPY content of the catalyst

The PPY content is a key factor that affects the ORR pathway and directly affects the formation of the catalytic sites (—C=N—C= and Co—Nx) on the PPY-modified catalysts. Fig. 6 shows the N 1s, Co $2p_{1/2}$, and Co $2p_{3/2}$ core level spectra of the $Co(OH)_2$-PPY-BP samples with different PPY contents. When the PPY content in $Co(OH)_2$-PPY-BP is increased, the calculated relative proportions of the N_I component for the PPY0, PPY10, PPY20, and PPY30 samples are 0%, 27.4%, 42.0%, and 56.0%, respectively. The relative proportion of the N_I component increases with the PPY content. The calculated relative Co surface concentrations for PPY0, PPY10, PPY20, and PPY30 samples are 0.9%, 1.7%, 1.5%, and 2.2%, respectively, indicating the increase in the relative Co surface concentration with increasing PPY content (Fig. 6b). However, the calculated relative proportions of the N_{II} component for the PPY0, PPY10, PPY20, and PPY30 samples are 0%, 19.9%, 15.2%, and 15.5%, respectively. The relative proportion of the N_{II} component initially increases when the PPY content is below 10 wt.% and then decreases when the value exceeds 10 wt.% (Fig. 6a).

Fig. 7 shows the RDE voltammograms of the catalysts supported on glass carbon electrodes, namely, the PPY0/GC, PPY10/GC, PPY20/GC, and PPY30/GC electrodes, at rotation rates of 200, 400, 600, and 800 rpm, respectively. The K–L plots obtained from the RDE voltammograms of $Co(OH)_2$-PPY-BP with different PPY contents using limiting currents at −0.6 V (Fig. 7) are shown in Fig. 8a. The relationship between n and $-I_l$ in the ORR with different PPY contents is shown in Fig. 8b. The absolute value of I_l initially increases as the PPY content increases; however, n decreases when the PPY content in the catalyst exceeds 20 wt.%. The XPS results

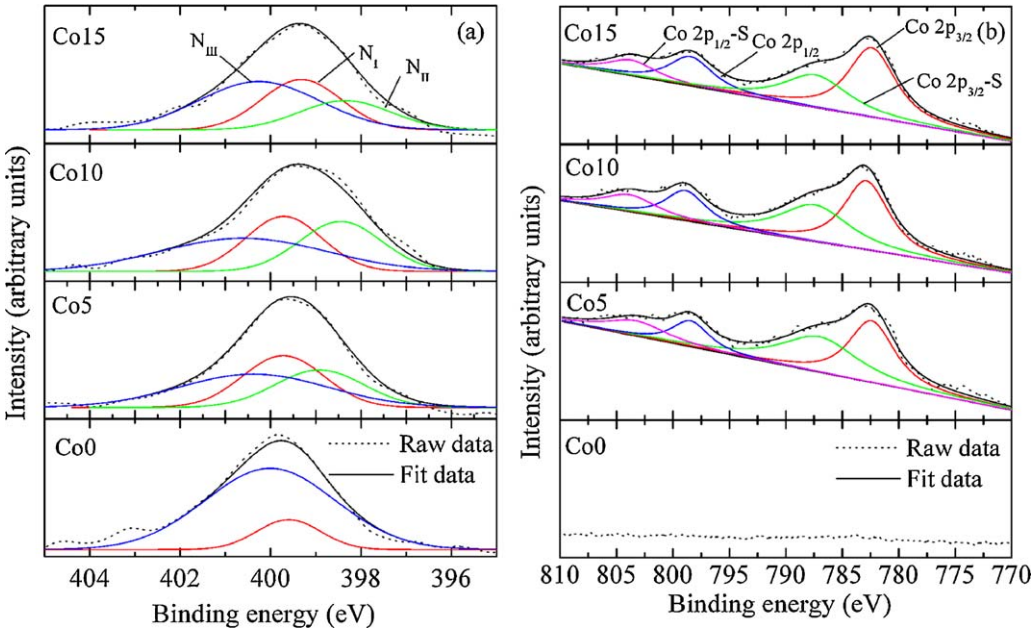

Fig. 2. XPS (a) N 1s and (b) Co 2p spectra for the $Co(OH)_2$-PPY-BP catalysts with different Co contents.

suggest that increasing the PPY content leads to an increase in the Co—N*x* density (N_{II}), which in turn increases *n*. However, a further increase in the PPY content does not lead to the production of more Co—N*x* sites. Therefore, the catalytic activity of $Co(OH)_2$-PPY-BP decreases when the PPY content exceeds 20 wt.%. The *n* values of PPY0, PPY10, PPY20, and PPY30 are 3.7, 3.8, 3.5, and 3.0 (Fig. 8b), respectively. The relative intensities of N_I to N_{II} in PPY10, PPY20, and PPY30 are N_I:N_{II} = 1.4, 2.8, and 3.6, respectively. The value of *n* coincidently decreases with the increase in the relative intensities of N_I to N_{II}, revealing that the four-electron transfer reaction gradually tends to lose its dominance in the ORR process. Therefore, the catalytic site competition between Co—N*x* (N_{II}) and —C=N—C= (N_I) dictates the overall electron number of $Co(OH)_2$-PPY-C toward ORR.

3.4. Catalytic activity of $Co(OH)_2$-PPY-C

The catalytic activity of $Co(OH)_2$-PPY-C is affected by many factors, such as abundance of the catalytic sites (Co—N*x* and —C=N—C=) on the catalyst surface and the ratio of Co—N*x* to —C=N—C=. The carbon support, $Co(OH)_2$, and the PPY contents affect the number of catalytic sites and the ratio of Co—N*x* to

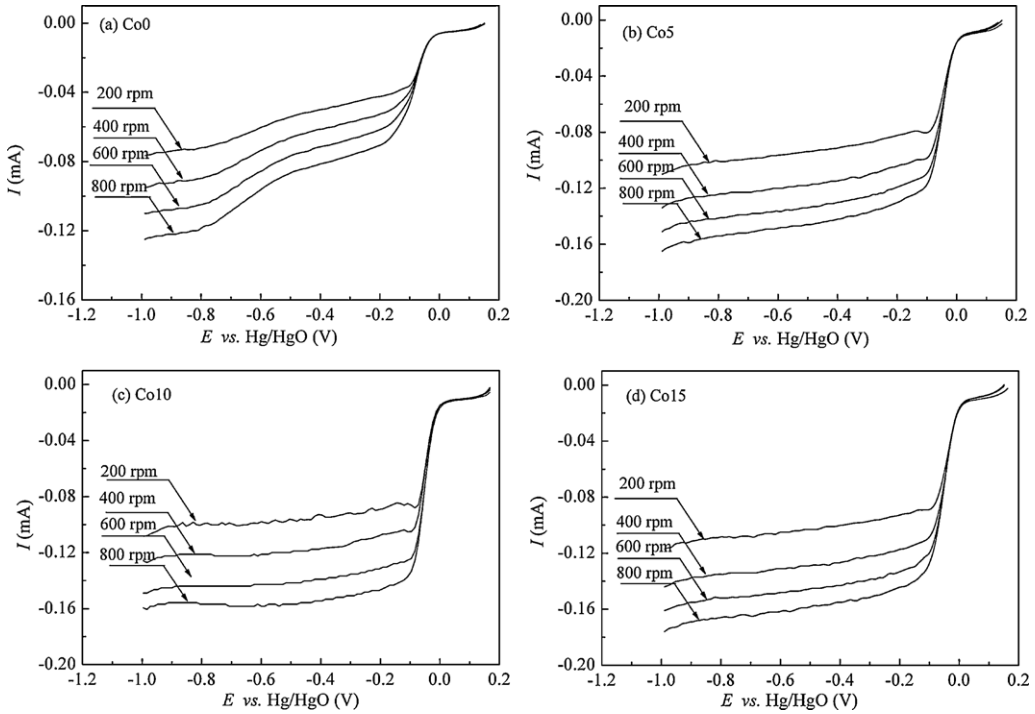

Fig. 3. Rotating disk electrode (RDE) voltammograms of the oxygen reduction reaction (ORR) on the (a) Co0/GC, (b) Co5/GC, (c) Co10/GC, and (d) Co15/GC electrodes in an O_2-saturated 0.1 M KOH solution. Scan rate: 10 mV s^{-1}.

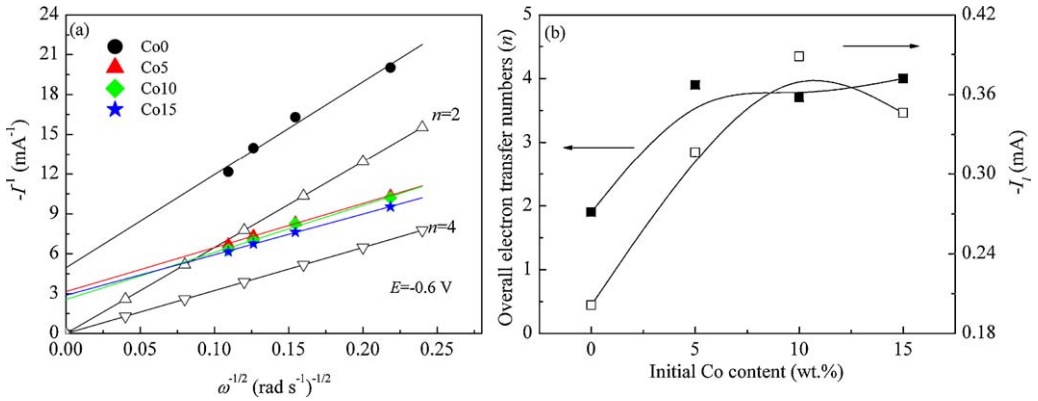

Fig. 4. (a) Koutecky–Levich (K–L) plots of the $Co(OH)_2$-PPY-BP catalysts with different Co contents (theoretical slopes for the two- and four-electron processes are also given). The data were taken at −0.6 V (vs. Hg/HgO) from Fig. 3. (b) ORR electrons (n) and the absolute value of kinetically limiting current ($-I_l$) of the $Co(OH)_2$-PPY-BP catalysts with different Co contents.

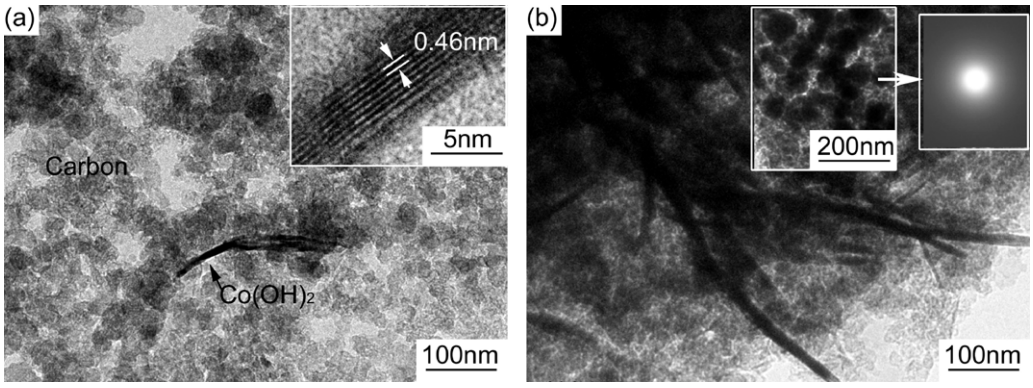

Fig. 5. Transmission electron microscopy (TEM) images of the as-prepared (a) Co5 and (b) Co15. The inset in (a) is the a high-resolution TEM image of $Co(OH)_2$, and the inset in (b) shows the noncrystalline Co particles and their corresponding selected area electron diffraction patterns.

—C═N—C═ on the catalyst surface. The LSVs of ORR on $Co(OH)_2$-PPY-SP and $Co(OH)_2$-PPY-BP are shown in Fig. 9a. The LSVs of the $Co(OH)_2$-PPY-BP/GC electrode recorded in N_2- or O_2-saturated 0.1 M KOH solutions are shown in the inset of Fig. 9a. No obvious reduction peak is observed in the N_2-saturated 0.1 M KOH solution. In the presence of O_2, the $Co(OH)_2$-PPY-BP catalyst has a higher onset ORR potential (0.09 V) and peak current (0.115 mA) than $Co(OH)_2$-PPY-SP (0.07 V and 0.05 mA). The XPS results suggest that the increase in the number of catalytic sites ($N_I + N_{II}$) of $Co(OH)_2$-PPY-BP contributes to its higher ORR peak current compared to $Co(OH)_2$-PPY-SP. After durability testing in DBFC for 50 h (Fig. 10), the Co—Nx sites of $Co(OH)_2$-PPY-SP disappear, but those of $Co(OH)_2$-PPY-BP remain. This result verifies that Co—Nx (N_{II}) on the $Co(OH)_2$-PPY-C catalysts is an important catalytic site for ORR. On the other hand, PPY-modification on carbon can increase the onset ORR potential of $Co(OH)_2$-PPY-BP (Fig. 9c).

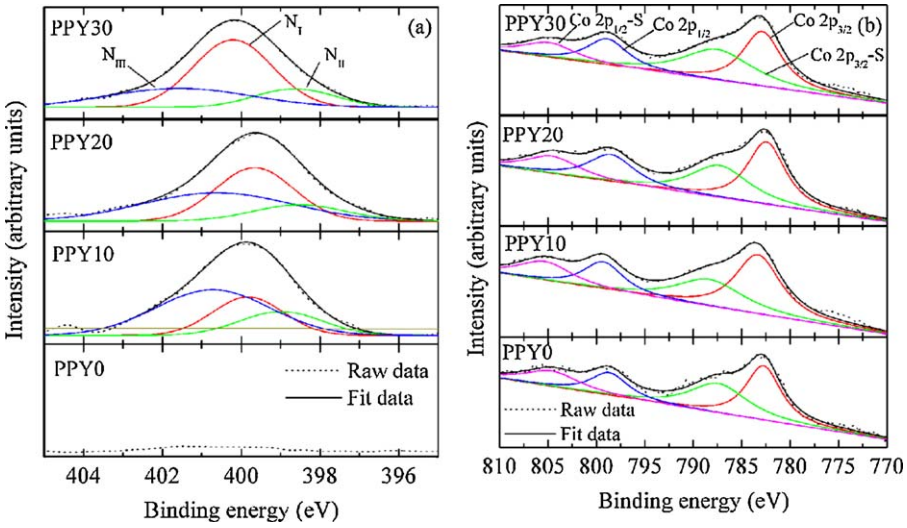

Fig. 6. XPS (a) N 1s and (b) Co 2p spectra for the $Co(OH)_2$-PPY-BP catalysts with different polypyrrole (PPY) contents.

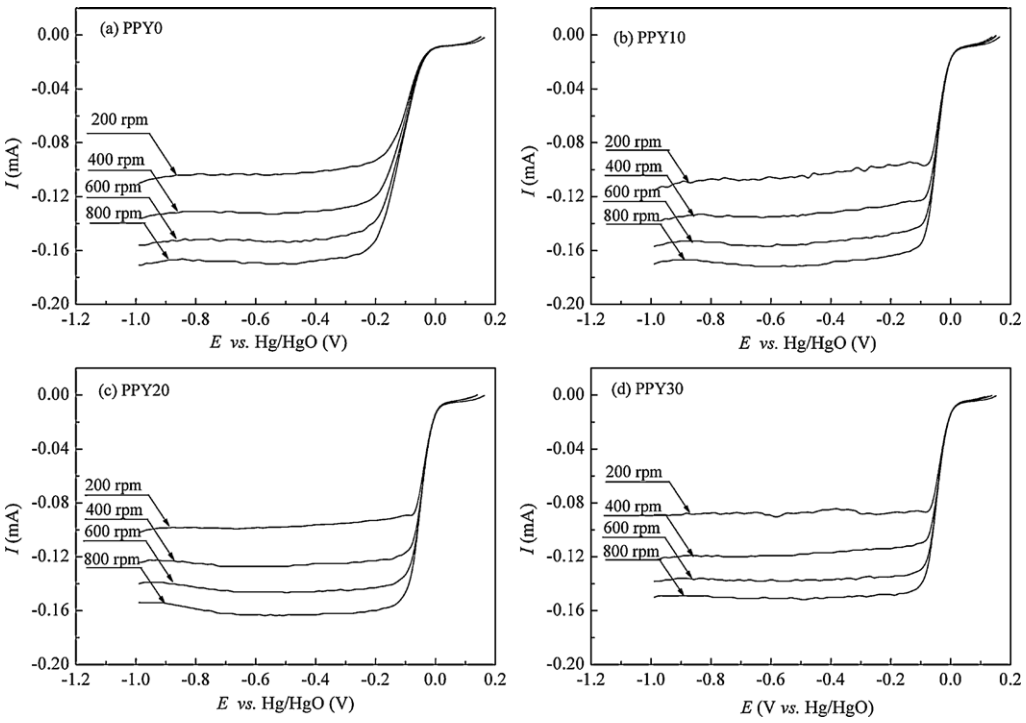

Fig. 7. RDE voltammograms of ORR on the (a) PPY0/GC, (b) PPY10/GC, (c) PPY20/GC, and (d) PPY30/GC electrodes in an O_2-saturated 0.1 M KOH solutions. Scan rate: 10 mV s^{-1}.

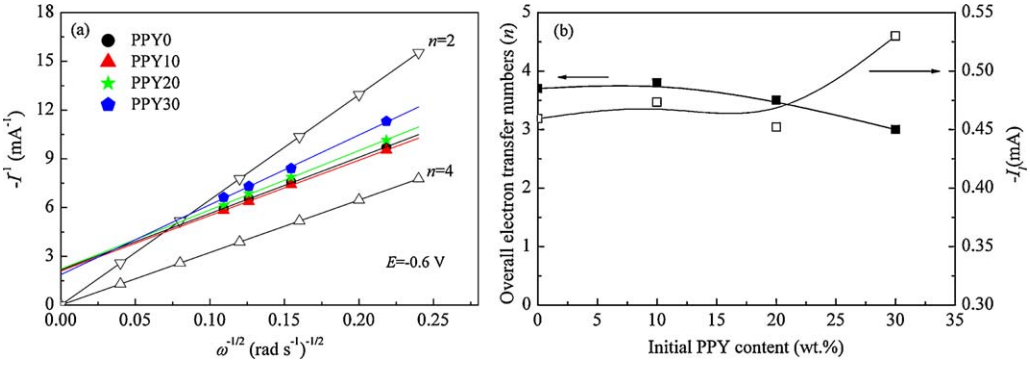

Fig. 8. (a) K–L plots of the $Co(OH)_2$-PPY-BP catalysts with different PPY contents (theoretical slopes for the two- and four-electron processes are also given). The data were taken at −0.6 V (vs. Hg/HgO) from Fig. 7. (b) n and $-I_l$ of the $Co(OH)_2$-PPY-BP catalysts with different PPY contents.

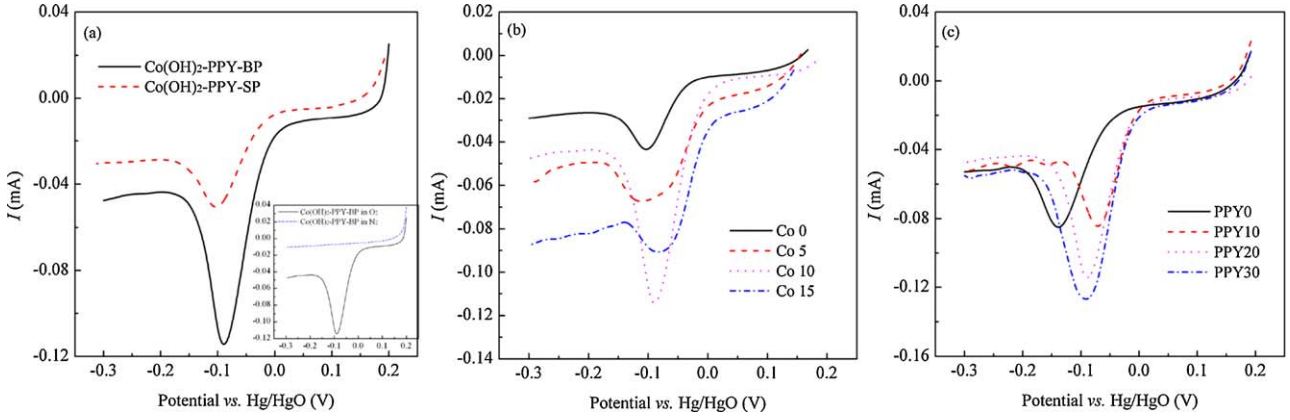

Fig. 9. Linear sweep voltammograms (LSVs) of (a) the $Co(OH)_2$-PPY-SP and $Co(OH)_2$-PPY-BP catalysts in an O_2-saturated 0.1 M KOH solution; the inset shows the LSVs of the $Co(OH)_2$-PPY-BP/GC electrode recorded in N_2- or O_2-saturated 0.1 M KOH solution; (b) LSVs of the $Co(OH)_2$-PPY-BP catalysts with different Co contents in an O_2-saturated 0.1 M KOH solution, and (c) LSVs of the $Co(OH)_2$-PPY-BP catalysts with different PPY contents in an O_2-saturated 0.1 M KOH solution.

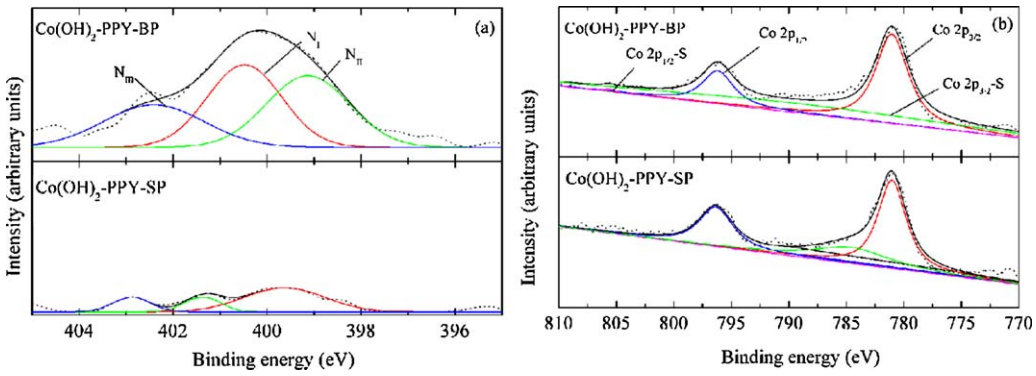

Fig. 10. XPS (a) Co 2p and (b) N 1s spectra for the $Co(OH)_2$-PPY-SP and $Co(OH)_2$-PPY-BP catalysts after durability testing in a direct borohydride fuel cell (DBFC) for 50 h at a current density of 50 mA cm^{-2}.

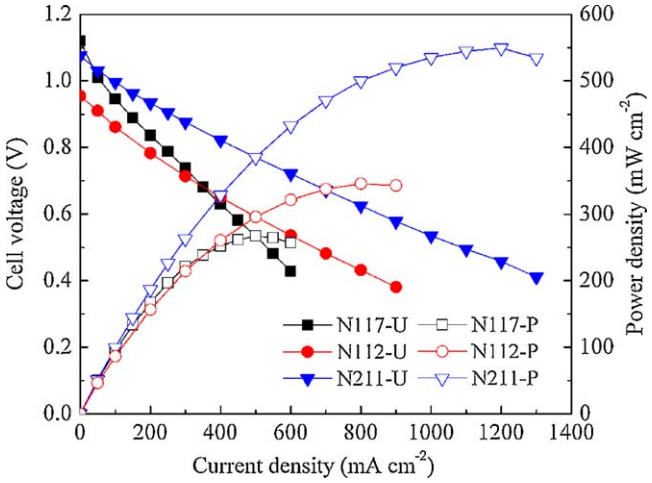

Fig. 11. Cell performance of DBFC using Co10 as the cathode catalyst and Nafion 117, 112, or 211 membrane as the electrolyte, operated at 80 °C. Cathode catalyst loading: 5 mg cm^{-2}; humidified O_2 at 150 mL min^{-1} flow rate (0.3 MPa); anode: 10 mg cm^{-2} Ni–Pt/C catalyst; fuel: 5 wt.% of $NaBH_4$ and 10 wt.% of NaOH solution at 50 mL min^{-1} fuel flow rate.

A previous study [21] showed that the catalyst activity measured in RDE corresponds to the catalyst performance in the fuel cell. The Co10 catalyst exhibits the highest electrocatalytic activity toward ORR among the test samples (Fig. 9b). The polarization curves and the corresponding power densities of DBFC using Co10 as the cathode catalyst are shown in Fig. 11. The maximum power densities of 267, 345, and 550 mW cm^{-2} are achieved at 80 °C when N117, N112, and N211 are used as the electrolyte, respectively. These values are higher than those of the previously reported representative DBFC [22–25].

4. Conclusions

Electrochemical evaluation and physical characterization were conducted to investigate the relationship between the catalyst composition and the ORR mechanism. The carbon support affects the formation of the catalytic sites. XPS results suggest that Co—N*x* and —C=N—C= are responsible in enhancing the ORR kinetics. The Co—N*x* and —C=N—C= sites drive the four- and two-electron transfer ORR, respectively. The overall electron number of ORR on the $Co(OH)_2$-PPY-C catalysts is determined by the competition between the Co—N*x* and —C=N—C= sites. The catalytic activity of $Co(OH)_2$-PPY-C can be improved by optimizing its carbon support, as well as its PPY and $Co(OH)_2$ contents.

Acknowledgments

This work is financially supported by the National Natural Science Foundation of China, Grant Nos. 20976156 and 21006090; special grade of China Postdoctoral Science Foundation, Grant No. 201003719; the Zhejiang Provincial Natural Science Foundation of China, Grant No. Z4110126; the Doctoral Fund from the Education Ministry of China (20100101110042); and the Fundamental Research Funds for the Central Universities.

References

[1] B. Wang, J. Power Sources 152 (2005) 1–15.
[2] Z.P. Li, B.H. Liu, J. Appl. Electrochem. 40 (2010) 475–483.
[3] L. Zhang, K. Lee, C.W.B. Bezerra, J. Zhang, J. Zhang, Electrochim. Acta 54 (2009) 6631–6636.
[4] M. Lefevre, E. Proietti, F. Jaouen, J.P. Dodelet, Science 324 (2009) 71–74.
[5] R. Bashyam, P. Zelenay, Nature 443 (2006) 63–66.
[6] C.W.B. Bezerra, L. Zhang, K. Lee, H. Liu, A.L.B. Marques, E.P. Marques, H. Wang, J. Zhang, Electrochim. Acta 53 (2008) 4937–4951.
[7] J.S. Spendelow, A. Wieckowski, Phys. Chem. Chem. Phys. 9 (2007) 2654–2675.
[8] F.H.B. Lima, J.F.R. de Castro, E.A. Ticianelli, J. Power Sources 161 (2006) 806–812.
[9] Z.X. Liu, Z.P. Li, H.Y. Qin, B.H. Liu, J. Power Sources 196 (2011) 4972–4979.
[10] H.Y. Qin, Z.X. Liu, S.J. Lao, J.K. Zhu, Z.P. Li, J. Power Sources 195 (2010) 3124–3129.
[11] H.Y. Qin, Z.X. Liu, W.X. Yin, J.K. Zhu, Z.P. Li, J. Power Sources 185 (2008) 909–912.
[12] H.Y. Qin, Z.X. Liu, L.Q. Ye, J.K. Zhu, Z.P. Li, J. Power Sources 192 (2009) 385–390.
[13] H.Y. Qin, S.J. Lao, Z.X. Liu, J.K. Zhu, Z.P. Li, Int. J. Hydrogen Energy 35 (2010) 1872–1878.
[14] M. Yuasa, A. Yamaguchi, H. Itsuki, K. Tanaka, M. Yamamoto, K. Oyaizu, Chem. Mater. 17 (2005) 4278–4281.
[15] V. Nallathambi, J.W. Lee, S.P. Kumaraguru, G. Wu, B.N. Popov, J. Power Sources 183 (2008) 34–42.
[16] A.J. Bard, L.R. Faulkner, Electrochemical Methods: Fundamentals, Application, 2nd ed., John Wiley & Sons, Inc., New York, 2001, p. 341.
[17] D. Zhang, D. Chi, T. Okajima, T. Ohsaka, Electrochim. Acta 52 (2007) 5400–5406.
[18] F. Charreteur, S. Ruggeri, F. Jaouen, J.P. Dodelet, Electrochim. Acta 53 (2008) 6881–6889.
[19] C.Z. Deng, M.J. Dignam, J. Electrochem. Soc. 145 (1998) 3507–3512.
[20] G. Wu, M.A. Nelson, N.H. Mack, S.G. Ma, P. Sekhar, F.H. Garzon, P. Zelenay, Chem. Commun. 46 (2010) 7489–7491.
[21] M. Lefevre, J.P. Dodelet, P. Bertrand, J. Phys. Chem. B 104 (2000) 11238–11247.
[22] E. Gyenge, M. Atwan, D. Northwood, J. Electrochem. Soc. 153 (2006) A150–A158.
[23] J. Ma, Y. Sahai, R.G. Buchheit, J. Power Sources 195 (2010) 4709–4713.
[24] Z.P. Li, B.H. Liu, J.K. Zhu, S. Suda, J. Power Sources 163 (2006) 555–559.
[25] B.H. Liu, Z.P. Li, J. Power Sources 187 (2009) 291–297.